

## Wetting and structure of a fluid in a spherical cavity

Ioannis A. Hadjiagapiou\*

*Solid State Physics Section, Department of Physics, University of Athens, Panepistimiopolis, Zografos GR-157 84, Athens, Greece*

(Received 22 December 2000; revised manuscript received 23 July 2001; published 18 January 2002)

The equilibrium local densities, structure, and wetting of a one-component fluid in a spherical cavity, of variable radius  $R$ , are determined, using density-functional theory, as functions of two parameters characterizing the system: the radius  $R$  and the cavity/fluid potential parameter  $\epsilon_w$ . The cavity acts as an external potential  $V_{\text{ext}}(r)$  on the molecules of the confined fluid, the particles of which are of constant diameter  $d$ . The equilibrium density profile, as a result of strong confinement, develops peaks in the center of the cavity and/or close to the pore wall and, in certain situations, in other intermediate points; the cavity can also be liquid full, capillary condensation.

DOI: 10.1103/PhysRevE.65.021605

PACS number(s): 68.08.Bc, 68.15.+e, 68.43.De

### I. INTRODUCTION

Wetting of planar or curved surfaces and porous media by fluids has received considerable attention in recent years because of its industrial (chromatography, membrane transport, adhesion, lubrication, foams) and theoretical significance as an application of the statistical physics of nonhomogeneous systems. These inhomogeneous classical fluids can be studied via density-functional theory (DFT), a very efficient tool for dealing with interfacial phenomena and nonhomogeneous fluids [1,2]. The DFT formulation has successfully been applied to adsorption, wetting, layering transitions, and capillary condensation at planar and nonplanar substrates. The key point in DFT is attributed to the grand-potential density functional  $\Omega_V[\rho]$ , wherein, *ad hoc*, assumptions are introduced, motivated by physical reasoning, to render the intrinsic Helmholtz free-energy functional  $\mathcal{F}[\rho]$  of the inhomogeneous fluid calculable. These are introduced, reflecting the situation at hand, either by the local density approximation or weighted density approximation, considering the geometrical characteristics of the system for the calculation of  $\Omega_V[\rho]$ .

In the current case, the DFT formulation will be applied to the study of a gas phase enclosed in a spherical cavity (an infinitely thin solid shell) of variable radius  $R$ . In general, the thermodynamical properties of a fluid confined in the cavities (pores) of a solid material are altered (sometimes, even those of the host material) as compared to those of a similar bulk counterpart, i.e., displacement of the location of the bulk fluid phase boundaries, shifted bulk transitions, and competition between surface transitions, since small and very small cavities can hold a few adsorbed particles, making the enclosed fluid highly spatially inhomogeneous. In such systems, the packing constraints are very pronounced because of the strong confinement. The pores of the host material can be of any shape, but, on computational grounds, they are chosen to be slitlike, cylindrical, or spherical.

The cylindrical pore is of infinite length and finite radius, the slitlike consists of two parallel walls of infinite area and separated by a finite distance; in both cases, the fluid can be

in contact with a reservoir at constant temperature  $T$  and chemical potential  $\mu$  implying an open system; in either case, the appropriate ensemble is the grand canonical. In the current case, the considered spherical cavity is an element of an ensemble of similar cavities connected to each other and to the external world by windows and/or narrow channels, enabling them to exchange particles among themselves and with an external reservoir of constant temperature  $T$  and chemical potential  $\mu$ , resulting in a net flow of particles through this pore arrangement; consequently, the proper ensemble is the grand canonical. This arrangement of pores is found in zeolites [3], which are used as membranes for separating gas or liquid mixtures, causing adsorption of particles by their pores [4]. An alternative choice, is to consider that the bulk phase of the enclosed phase inside the zeolites' pores is the homogeneous phase that would be found if the external force, for maintaining the inhomogeneity, is removed [5]. Although the previous assumption is adopted, another contemplation of the system is to consider the spherical cavity as closed, confining a constant number of particles, specified *a priori*, and study it using the methods of the canonical ensemble [6]. An important point that is raised is the equivalence of the results from the two approaches, grand-canonical and canonical, a crucial problem of statistical mechanics. Since the volume occupied by the cavity and each particle is finite, the number of enclosed particles is always finite, however, within the grand-canonical ensemble it can vary continuously (although it cannot exceed a maximum value specified by the repulsive interactions, excluded-volume effect), resulting in a variety of configurations inside the cavity, in contradistinction to the canonical-ensemble description wherein the number of enclosed particles is specified *a priori* and remains always constant resulting in a single configuration, for a given temperature. The grand-canonical ensemble might produce the same fluid structure as that by canonical ensemble, in a similar cavity, when the instantaneous number of particles in the grand-canonical ensemble coincides with the corresponding number in the canonical ensemble.

In the statistical mechanics for bulk systems, the probability  $P(N)$  that a macroscopic system, in the grand-canonical ensemble, has  $N$  particles exhibits an extremely sharp maximum at  $N = \langle N \rangle$  and, in this case, the mean value  $\langle N \rangle$  coin-

\*Email address: ihatziag@phys.uoa.gr

cides with the most probable  $N^*$ ,  $\langle N \rangle = N^*$ , so that the considered grand-canonical-ensemble systems are those whose number of particles equals  $\langle N \rangle$  and coincides with the fixed number of particles  $N$  in the canonical ensemble, equivalence of ensembles. This coincidence implies that the chemical potential  $\mu$  is fixed so that the average number of particles equals  $N$ .

Most studies have been focused on fluids adsorbed on planar substrates, while previous studies of fluids inside pores dealt with adsorption of hard spheres in a hard spherical cavity [5–10], cylindrical pores [9], narrow channels [11].

The current study is now extended to include attractive interactions in a one-component fluid system composed of  $N$  spherical particles (of diameter  $d$ ) which, initially, are considered to be hard spheres and an additional attractive interaction is introduced. These are enclosed in a spherical cavity of radius  $R$  ( $R \geq d/2$ ) with its center at the origin of axes. The boundary of the cavity is impenetrable and each particle interacts with an element of the cavity boundary with an attractive interaction, so the total interaction between a fluid particle and the cavity is

$$V_{\text{ext}}(\vec{r}) = n_S \int_S w_{WF}(|\vec{r} - \vec{r}'|) d\vec{r}', \quad (1.1)$$

where  $w_{WF}(|\vec{r} - \vec{r}'|)$  is the pairwise interaction potential between a fluid molecule at  $\vec{r}$  and a wall molecule at  $\vec{r}'$ ,  $n_S$  wall density and  $S$  the area of cavity's boundary. The potential (1.1) acts as an external potential for the  $N$ -particle system in the cavity, inducing the inhomogeneity in the fluid. The study considers a suitable grand-potential density functional, adapted for the current model, from which the equilibrium density profile results via the minimum grand-potential principle; the structure, thermodynamic properties, and wetting are also investigated. Similar models have been applied successfully to planar [12,13], spherical [14] substrates, and spherical drops [15].

The state point chosen corresponds to a homogeneous bulk vapor phase, of density  $\rho_b$  at reduced temperature  $T^* \equiv T/T_c = 0.8$ ,  $T_c$  is the bulk critical temperature and packing fraction  $\eta_b = \pi/6 d^3 \rho_b = 0.021\,717\,8$

The paper is arranged as follows: In Sec. II the system is defined through a density-functional grand potential. The numerical calculations are in Sec. III and the discussion in Sec. IV.

## II. THEORY

### A. Thermodynamic description

When a single planar solid substrate exerts an attractive force on the particles of a bulk gas phase, under certain conditions, some of the particles will be adsorbed by the substrate, forming a liquidlike film on it and causing wetting of the substrate. The thickness  $\ell$  of the film, on approaching saturation, can be finite (partial wetting) or infinite (complete wetting [12,13]). If the gas phase is enclosed in a pore (cylindrical, spherical, slitlike) of a porous solid (host phase), then, in addition to the wetting transition, other ones can

appear, as the capillary condensation. The latter case appears even if the chemical potential or pressure is less than its value at saturation; in this case, gas particles condense to form a dense liquidlike state inside the pore, liquid-full pore. The reduction in condensation chemical potential or pressure results from the attractive forces between gas particles and the surrounding pore walls; this early condensation of the gas phase can be considered as a shift of the bulk coexistence gas-liquid line due to confinement effects.

The phase equilibria of an enclosed fluid in a spherical cavity, for sufficiently large  $R$ , can be determined by thermodynamic arguments. The temperature  $T$  is smaller than the bulk critical temperature  $T_c$  ( $T < T_c$ ) and the bulk chemical potential  $\mu$  is smaller than that at saturation  $\mu_{\text{sat}}$  ( $\mu < \mu_{\text{sat}}$ ) so that the bulk fluid is gas. The grand potential  $\Omega_V$  is divided into two contributions, the bulk and surface, and the enclosed fluid adopts the configuration minimizing  $\Omega_V$ . When the wall-fluid attraction is relatively strong, a liquidlike film, of thickness  $\ell$ , intrudes between the wall and the gas phase, so that the liquid phase wets the wall and the respective grand potential  $\Omega_{gL}$  is

$$\begin{aligned} \frac{\Omega_{gL}}{4\pi} = & -\frac{p}{3}(R - \ell)^3 - \frac{p_L^+}{3}(3\ell R^2 - 3\ell^2 R + \ell^3) + \gamma_{wL}R^2 \\ & + \gamma_{gL}(R - \ell)^2, \end{aligned} \quad (2.1)$$

where  $p_L^+$  is the pressure of the metastable liquid with density  $\rho_L^+$  at the same value of  $\mu$  and  $\gamma_{wL}$ ,  $\gamma_{gL}$  are the wall-liquid and gas-liquid surface tensions, respectively. However, if the wall-fluid attractive interaction becomes stronger, the enclosed fluid condenses abruptly to a liquid configuration (liquid-full pore); the respective grand potential  $\Omega_L$  is

$$\frac{\Omega_L}{4\pi} = -\frac{R^3}{3} p_L^+ + R^2 \gamma_{wL}. \quad (2.2)$$

Coexistence is possible when

$$\Omega_{gL} = \Omega_L. \quad (2.3)$$

Substituting Eq. (2.1) and Eq. (2.2) into Eq. (2.3),

$$p - p_L^+ = \frac{3\gamma_{gL}}{R - \ell}, \quad (2.4)$$

which is similar to the Laplace expression for the pressure difference across a spherical surface, whose effective radius of curvature is  $(2(R - \ell)/3)$ . When Eq. (2.4) holds, it signals the beginning of condensation; however, its drawback is that there is not a systematic way for calculating the thickness  $\ell$  of the wetting layer.

### B. Density profile

As was mentioned in the introduction, one of the most widely used theoretical descriptions of inhomogeneous fluids is the density-functional theory, which relies on a proper choice of the grand-potential functional  $\Omega_V[\rho(\mathbf{r})]$ ; consequently the key step is to specify a form for  $\Omega_V[\rho(\mathbf{r})]$  that is

tractable and more or less accurate. In general, the grand-potential functional of an inhomogeneous one-component fluid in the presence of an external field  $V_{\text{ext}}(r)$ , representing the substrate, is [1,2]

$$\Omega_V[\rho(\vec{r})] = \int_V \left\{ f_{\text{hs}}[\rho(\vec{r})] + \frac{1}{2} \rho(\vec{r}) \int_V \rho(\vec{r}') \Phi_{FF} + [V_{\text{ext}}(\vec{r}) - \mu] \rho(\vec{r}) \right\} d\vec{r}, \quad (2.5)$$

where  $\mu$  the bulk vapor chemical potential and  $V$  the volume of the system. The repulsive force contribution to the Helmholtz free energy is treated in the local-density approximation (LDA) in that  $f_{\text{hs}}[\rho(\vec{r})]$  is the Helmholtz free-energy density of a uniform hard-sphere fluid at density  $\rho(\vec{r})$ ,  $r = |\vec{r}|$  is the distance to the center of the cavity. Although LDA fails to describe the oscillatory behavior of the density profile at strongly attractive walls, it gives reasonable results for the surface tension, adsorption, and the density profile of the free liquid-vapor interface. The long-range attractive forces between fluid molecules are treated in the mean-field approximation,  $\Phi_{FF}(\vec{r})$  is the attractive part of the pairwise potential between two fluid molecules  $r$  distant apart. The equilibrium density  $\rho(\vec{r})$  of the inhomogeneous fluid is obtained by minimizing Eq. (2.5) through the variational principle  $\delta\Omega_V[\rho(\vec{r})]/\delta\rho(\vec{r}) = 0$ ,

$$\mu = V_{\text{ext}}(\vec{r}) + \mu_{\text{hs}}[\rho(\vec{r})] + \int_V \rho(\vec{r}') \Phi_{FF}(|\vec{r} - \vec{r}'|) d\vec{r}', \quad (2.6)$$

where  $\mu_{\text{hs}}[\rho(\vec{r})] = \partial f_{\text{hs}}[\rho(\vec{r})]/\partial\rho(\vec{r})$  is the chemical potential of a uniform hard-sphere fluid of density  $\rho(\vec{r})$ . Choosing the potentials  $V_{\text{ext}}(\vec{r})$  and  $\Phi_{FF}(\vec{r})$ , properly, the integral equation (2.6) can be converted to a functional nonlinear second-order differential equation with appropriate boundary conditions. The fluid-fluid potential is

$$\Phi_{FF}(r) = -(\alpha\lambda^3/4\pi)e^{-\lambda r}/\lambda r, \quad (2.7)$$

where  $\lambda$  is an inverse-range parameter and  $\alpha$  is given by

$$\alpha = - \int_V \Phi_{FF}(r) d\vec{r}. \quad (2.8)$$

If a wall molecule interacts with a fluid molecule via a potential of the form,  $\mathcal{W}_{WF}(r) = -C e^{-\lambda_{WF} r}/(\lambda_{WF} r)$ , where  $\lambda_{WF} = \lambda$  ( $\lambda_{WF}$  inverse-range parameter of the wall-fluid attractive interaction) and  $C$  are positive constants, then Eq. (1.1) gives

$$V_{\text{ext}}(r) = -\epsilon_W(\lambda R) e^{-(\lambda R)} \frac{\sinh(\lambda r)}{\lambda r}, \quad (2.9a)$$

where  $\epsilon_W$  is a new parameter characterizing the substrate and proportional to  $n_s$  and  $C$ ; it is a measure of the well depth for the wall-fluid interaction. A feature of the potential (2.9a) is that its strength (that part separated from the distance dependence,  $\epsilon_W(\lambda R) e^{-(\lambda R)}$ ) depends strongly on substrate's ra-

dius  $R$ ; this dependence has significant repercussions on the structure of films inside the cavity. In the limit  $r \rightarrow 0$ , Eq. (2.9a) takes the form

$$\lim_{r \rightarrow 0} V_{\text{ext}}(r) = -\epsilon_W(\lambda R) e^{-\lambda R}, \quad (2.9b)$$

while on the cavity boundary,  $r = R$ ,

$$V_{\text{ext}}(R) = -\frac{\epsilon_W}{2} [1 - e^{-2\lambda R}], \quad (2.9c)$$

which, for large  $R$ ,  $V_{\text{ext}}(R) \approx -\epsilon_W/2$ , i.e., independent of  $R$  the spherical substrate becomes equivalent to a planar one. Although the chosen interaction potentials are short ranged, they are not only suitable for numerical calculations, but they yield an immediate classification of the wetting classes [12,13] and provide the general characteristics of wetting phenomena and interfacial structure, sacrificing some degrees of quantitative accuracy.

The chosen short-range interaction potentials (2.7), (2.9a) have repercussions on the wetting behavior of the system, inducing first- or second- (continuous) order wetting transitions. This behavior depends on the inverse range parameters  $\lambda$  and  $\lambda_{WF}$ , characterizing the fluid-fluid (2.7) and wall-fluid (2.9a) interactions; if they are taken to be equal, the resulting wetting transitions are continuous, called short-range critical wetting because they are dominated by short-range forces [16], on the opposite case, the transitions can be first order or continuous depending on their ratio and the strength of the wall-fluid interaction [17,18]. Although critical wetting attracted much theoretical attention [1,2,19,20], it eluded experimental confirmation, it was observed by Ross, Bonn, and Meunier [21] in the binary liquid mixture of methanol and nonane. In this mixture, the film thickness of methanol on nonane increases continuously from thin to thick and the divergence of the thickness is logarithmic, consistent with the renormalization-group and mean-field calculations for short-range critical wetting [20,22].

If the interaction forces are long range (algebraic decay), the wetting transitions are, in general, first order; continuous wetting transitions can also occur, called long-range critical wetting transitions, observed for the first time in an experiment by Ragil *et al.* [23]; they observed, using ellipsometry, a continuous transition from a thin film of pentane on water to a thick one, on increasing temperature  $T$  from low values to a wetting temperature  $T_W \cong 53^\circ\text{C}$  when the adsorbed film diverges [16].

From the previous discussions, one concludes that the order of the wetting transition governs the evolution of the thickness of the wetting film; a first-order transition yields a

jump in film thickness when temperature  $T$  approaches  $T_W$ , while in a second-order transition films grow continuously as  $T$  approaches  $T_W$ .

For the sake of simplicity, all subsequent quantities and equations are transformed to dimensionless units,

$$\begin{aligned} \mu^* &\equiv \beta\mu, & p^* &\equiv \beta d^3 p, & R^* &\equiv \lambda R, & r^* &\equiv \lambda r, & \rho^* &\equiv \rho d^3 \\ \alpha^* &\equiv \beta\alpha/d^3 = 11.102/T^*, & V_{\text{ext}}^* &\equiv \beta V_{\text{ext}}, \end{aligned} \quad (2.10)$$

although the asterisks will be suppressed,  $p$  is pressure,  $\beta = (k_B T)^{-1}$ , and  $k_B$  Boltzmann's constant.

Substituting the potentials (2.7) and (2.9a) into Eq. (2.6), and differentiating the resulting equation twice with respect to  $r$ , yields

$$\mu''_{\text{hs}}[\rho(r)] + \frac{2}{r} \mu'_{\text{hs}}[\rho(r)] - \mu_{\text{hs}}[\rho(r)] + \mu = -\alpha\rho(r), \quad (2.11)$$

the prime denotes derivative with respect to  $r$ . The final equation (2.11) depends only on the radial distance  $r$ , since both potentials are spherically symmetric. This is a functional differential equation, depending on  $\rho(r)$ ; its solution is uniquely defined if supplemented by appropriate boundary conditions. In the limit  $r \rightarrow 0$ , the solution is less well behaved, since at the origin  $r=0$  it is singular unless  $\mu'_{\text{hs}}(r)$  vanishes in that limit,

$$\lim_{r \rightarrow 0} \frac{\mu'_{\text{hs}}(r)}{r} = \lim_{r \rightarrow 0} \frac{d\mu'_{\text{hs}}(r)/dr}{dr/dr} = \lim_{r \rightarrow 0} \mu''_{\text{hs}}(r). \quad (2.12)$$

according to de l' Hopital rule, therefore, in the neighborhood of the origin (2.11) becomes

$$\lim_{r \rightarrow 0} \mu''_{\text{hs}}(r) = \frac{1}{3} [\mu_{\text{hs}}(r) - \mu - \alpha\rho(r)]. \quad (2.13)$$

Thus, the first boundary condition is

$$\mu'_{\text{hs}}(0) = 0, \quad (2.14)$$

and the other on the substrate,

$$\mu'_{\text{hs}}(R) = \epsilon_W - \left(1 + \frac{1}{R}\right) [\mu_{\text{hs}}(R) - \mu], \quad (2.15)$$

by differentiating Eq. (2.6) once with respect to  $r$  and evaluating it at  $r=R$ . The differential equation (2.11) in conjunction with the boundary conditions (2.14), (2.15) constitute the problem under consideration, which will be solved numerically since Eq. (2.11) is an implicit nonlinear second-order differential equation and cannot be solved analytically.

The calculation will be based on the Carnahan-Starling approximation for hard-spheres [24]; the pressure and chemical potential are, respectively,

$$\beta p_{\text{hs}}(\rho) = \rho \frac{1 + \eta + \eta^2 - \eta^3}{(1 - \eta)^3}, \quad (2.16a)$$

$$\beta \mu_{\text{hs}}(\rho) = \ln \eta + \frac{8\eta - 9\eta^2 + 3\eta^3}{(1 - \eta)^3}, \quad (2.16b)$$

where  $\eta = \pi\rho d^3/6$  is the packing fraction, which will be used as the dependent variable instead of the density  $\rho(r)$ .

Substituting Eq. (2.16b) into Eq. (2.11) yields

$$\eta''(r) = -\frac{2}{r} \eta'(r) - B_1(\eta) \eta'^2(r) - B_2(\eta) - B_3(\eta) \eta(r), \quad (2.17)$$

subject to the boundary conditions resulting from Eqs. (2.14) and (2.15),

$$\eta'(0) = 0, \quad (2.18a)$$

$$\begin{aligned} \eta'(R) &= \left\{ \epsilon_W - \left(1 + \frac{1}{R}\right) [\mu_{\text{hs}}(\eta(R)) - \mu] \right\} / \\ &A_1[\eta(R)], \end{aligned} \quad (2.18b)$$

where

$$\begin{aligned} A_1(\eta) &= \frac{\partial(\beta\mu_{\text{hs}})}{\partial\eta} = \frac{1}{\eta} + \frac{8-2\eta}{(1-\eta)^2}, & A_2(\eta) &= \frac{\partial A_1(\eta)}{\partial\eta} \\ &= -\frac{1}{\eta^2} + \frac{30-6\eta}{(1-\eta)^5}, \end{aligned} \quad (2.19a)$$

$$\begin{aligned} B_1(\eta) &= \frac{A_2(\eta)}{A_1(\eta)}, & B_2(\eta) &= \frac{\beta\mu - \beta\mu_{\text{hs}}(\eta)}{A_1(\eta)}, \\ B_3(\eta) &= \frac{6\alpha\beta}{\pi A_1(\eta)}. \end{aligned} \quad (2.19b)$$

Initially, the coexisting bulk densities  $\rho_V$  and  $\rho_L$  are calculated for various temperatures by solving the simultaneous equations

$$p(\rho_V) = p(\rho_L), \quad \mu(\rho_V) = \mu(\rho_L), \quad (2.20)$$

for  $T=0.8$ ,  $\rho_V=0.041478$ , and  $\rho_L=0.586731$ .

### III. RESULTS

The boundary value problem (2.17), (2.18) was solved numerically for a wide range of values of  $R$  and  $\epsilon_W$ ; the solution is the equilibrium density profile, which, depending on the values of  $R$  and  $\epsilon_W$ , displays various growth modes inside the cavity and the boundary various types of wetting behavior.

Initially, the density profiles for a cavity of radius  $R=4.5$  are evaluated for various values of  $\epsilon_W$ . The configurations, adopted by the confined fluid and possible phase transitions, depend on the specific value of  $\epsilon_W$  and the interparticle interactions.

For small values of  $\epsilon_W$  ( $\epsilon_W \leq 12.15$ ) a spherical liquid drop, of constant density  $\rho(0)$ , grows in the origin of the cavity, the rest part of the density profile is monotonically decreasing up to the pore boundary, resulting in a depletion

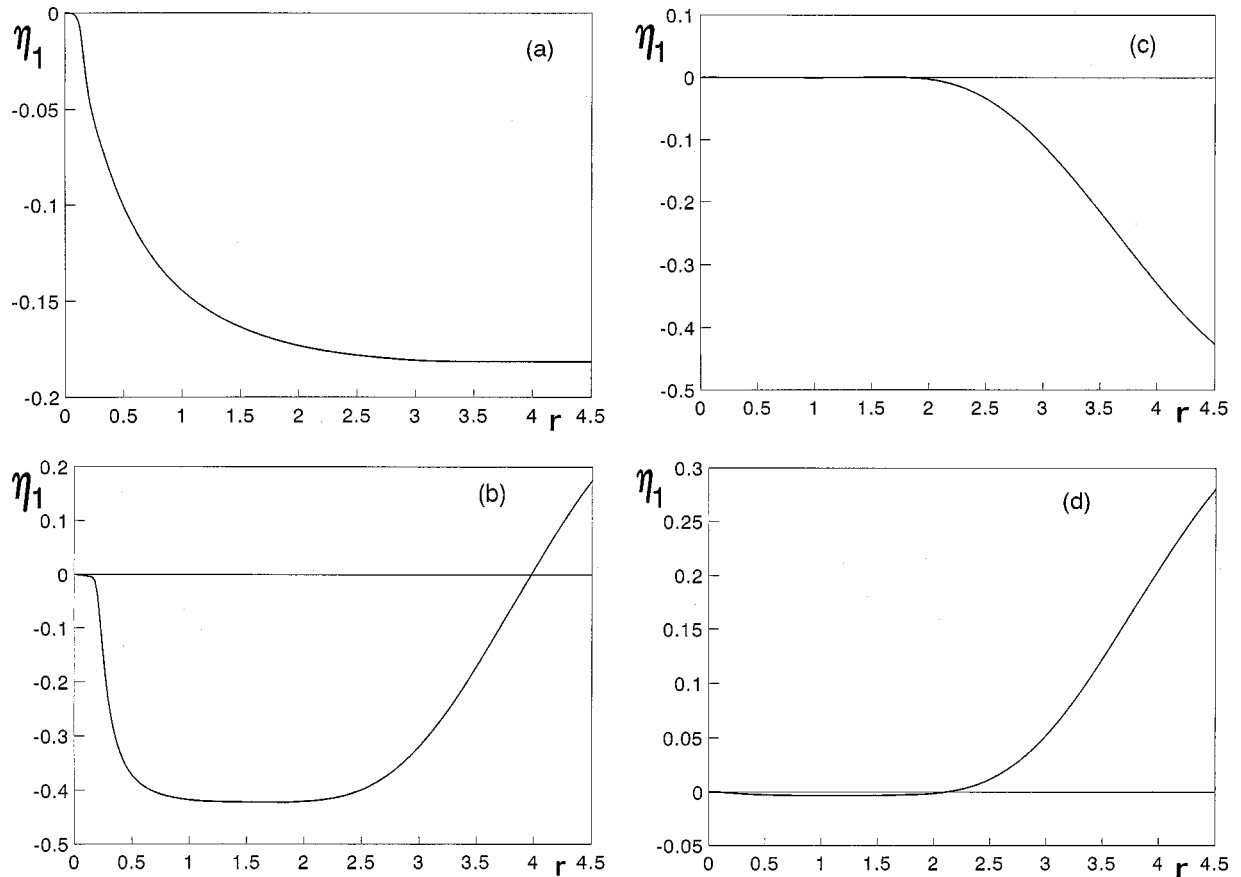


FIG. 1. Density profiles  $\eta_1(r) \equiv \eta(r) - \eta(0)$  vs radial distance  $r$  from the center of a spherical cavity of radius  $R=4.5$ , labeled by the parameter  $\epsilon_w$ , characterizing the wall-particle interaction: (a)  $\epsilon_w=12$ . The density profile consists of a thin liquid drop in the origin [density  $\eta_1(0)$ ] and a monotonically decreasing branch up to the boundary, with contact density  $\eta_{1w}$ , such that  $\eta_1(0) > \eta_{1w}$  so that the boundary is weakly wetted. (b)  $\epsilon_w=12.16$ . A thin liquid drop grows in the origin with density  $\eta_1(0)$ , the boundary is covered by a layer of adsorbed particles with contact density  $\eta_{1w} > \eta_1(0)$ , strong wetting of the boundary. (c)  $\epsilon_w=12.21$ . The density profile consists of a thick liquid drop in the origin (thin-thick transition) and a thin film at the boundary with  $\eta_{1w} < \eta_1(0)$ , weak wetting of the boundary. (d)  $\epsilon_w=12.22$ . The density profile consists of a thick liquid drop in the origin and a monotonically increasing branch up to the boundary which wets it [ $\eta_{1w} > \eta_1(0)$ ], the cavity is liquid full, capillary condensation. Both quantities are dimensionless. Remark. Each plot represents the difference [ $\eta_1(r) \equiv \eta(r) - \eta(0)$ ], so that the structure of the confined fluid is more evident.

of particles at the pore wall and a subsequent reduction of wetting (weak wetting). The local density at the pore wall ( $\rho_w$ , contact value) is an overall minimum, Fig. 1(a); however, for  $\epsilon_w=12.16$ , in addition to the thin liquid drop in the origin, the wall now attracts the particles favorably, forming a film at the wall, wherein the contact value exhibits an overall maximum [ $\rho(0) < \rho_w$ ] because of the strong accumulation of particles within the wall region, strong wetting (weak-strong wetting transition). The cavity region, between the two shells, presents a depletion of particles and the density profile attains a minimum value at an interior point, Fig. 1(b). For  $12.17 \leq \epsilon_w \leq 12.21$ , the density profile consists of two branches: the thin liquid drop in the origin, as in Figs. 1(a), 1(b), is transformed into a thick one, thin-thick transition, the second branch is monotonically decreasing up to the pore boundary implying weak-wetting (strong-weak wetting transition); the contact value is an overall minimum of the density profile, Fig. 1(c). For  $\epsilon_w=12.22$ , the thick liquid drop in the origin persists but the second branch of the density profile now increases steadily from the edge of the

central film to the wall where the density attains a maximum value [ $\rho(0) < \rho_w$ ] due to the strong attraction of the wall (strong wetting) resulting in a filling transition since the pore is now liquid full [capillary condensation, Fig. 1(a)]. For  $12.23 \leq \epsilon_w \leq 12.33$ , the weak-wetting situation reappears [ $\rho(0) > \rho_w$ ] with a thick liquid drop in the origin and the system returns to the situation depicted in Fig. 1(c). On further increasing  $\epsilon_w$ ,  $12.34 \leq \epsilon_w \leq 12.37$ , the system jumps from thick to thin liquid drop formation in the origin (thick-thin transition); the wall attracts strongly the particles [ $\rho(0) < \rho_w$ ] forming a film in the region of the boundary, strong wetting (weak-strong wetting transition); the contact value is a maximum while a depletion of particles appears in the region between the two branches as in Fig. 1(b) and, ultimately, for  $\epsilon_w \geq 12.38$  the system makes a transition to the initial case, Fig. 1(a), with a single thin liquid drop in the origin. The formation of the central liquid drops (mainly the thicker ones) is related to the strong potential field appearing in the pore center in certain circumstances, since the strength of the wall-particle potential  $V_{\text{ext}}(r)$  depends strongly on  $R$

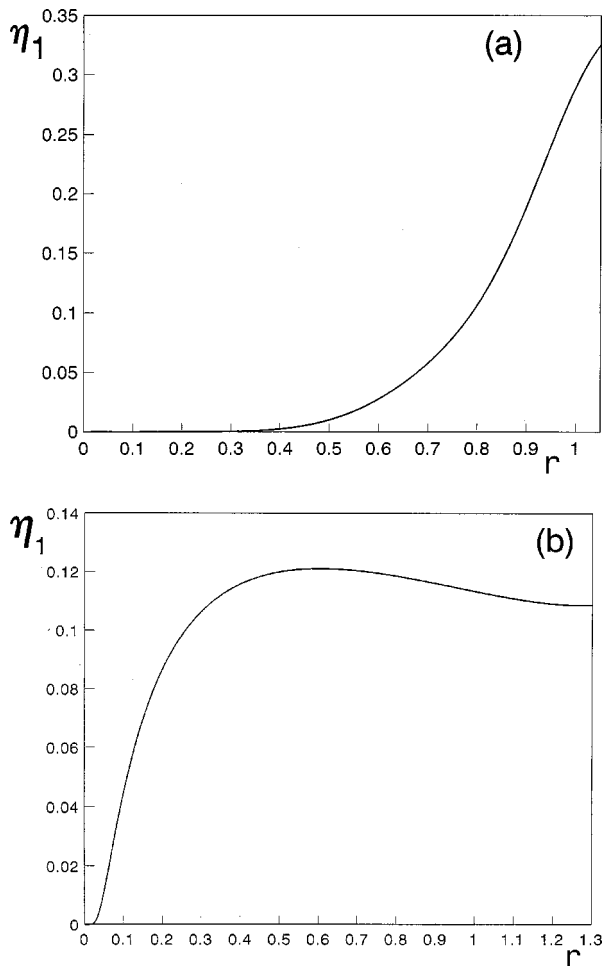


FIG. 2. Density profile  $\eta_1(r)$  vs radial distance  $r$  from the center of a spherical cavity of radius and wall parameter, respectively, (a)  $R=1.05$ ,  $\epsilon_w=1.64$ , (b)  $R=1.3$ ,  $\epsilon_w=1.3$ . In both cases, the cavities are liquid full, in case (b) the cavity, practically, is full of a constant-density liquid, while in case (a) the density profile consists of two branches, the one at the boundary corresponds to a denser phase. Both quantities are dimensionless.

(2.9a); in pore center  $V_{\text{ext}}(0) = -\epsilon_w R e^{-R}$  while at boundary  $V_{\text{ext}}(R) = -(\epsilon_w/2)(1 - e^{-2R})$  resulting in a weaker field at boundary for the  $R$ 's under consideration; for  $R \geq 6$ ,  $V_{\text{ext}}(R)$  becomes constant [ $V_{\text{ext}}(R) \cong -\epsilon_w/2$ ] and thus equivalent to a planar wall. This behavior of  $V_{\text{ext}}(r)$  favors, in some cases, the formation of a liquid drop in the origin, although the final equilibrium configuration is a result of all interactions.

Now, we proceed to examine the behavior of the fluid for various values of  $R$  and  $\epsilon_w$ . Both Figs. 2(a,b), where  $R=1.05$  and  $R=1.3$ , respectively, correspond to the liquid-full pore; however, they differ in the way the condensation occurs. In the former case, the liquid-full pore consists of a thick liquid drop in the origin and a monotonically increasing branch up to the wall because of the strong wall attraction and the contact value is a maximum of the overall densities; in the latter case, the pore is nearly full of the liquid phase, of almost constant density, except in the origin where a thin liquid drop grows, thus the condensation, practically, occurs

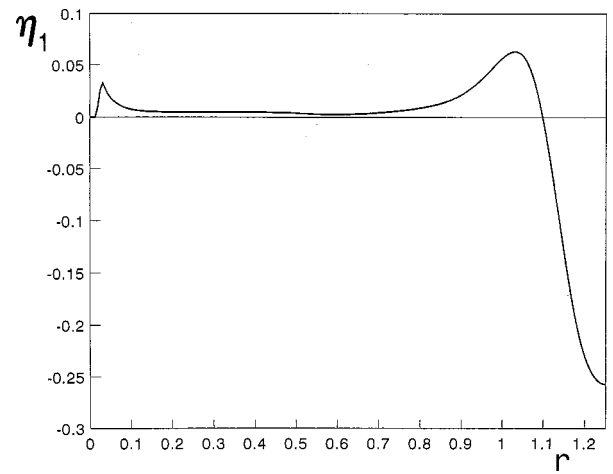


FIG. 3. Density profile  $\eta_1(r)$  vs radial distance  $r$  from the center of a spherical cavity of radius  $R=1.25$  and wall parameter  $\epsilon_w=1.3$ . The profile corresponds to two shells, one localized close to the center and the other to the boundary connected by a very long “bridge.” The wetting of the boundary is weak,  $\eta_1 w < \eta_1(0)$ . Both quantities are dimensionless.

in the whole pore [25]; the maximum value of the density profile occurs in an intermediate point and not at the wall, as usually in strong wetting, although this value does not differ significantly from the contact value. The structure of the confined fluid in the latter case is due to the stronger potential field in comparison to that in the former one. These two characteristic cases can be juxtaposed with the wetting of a planar wall; the former case, corresponds to the coexistence of two films, a thin and a thick (prewetting transition), while the latter one, corresponds to the complete wetting of the planar wall by a liquid film of infinite thickness [12].

However, this is not the only structure that can be observed in a cavity, more complex structures can also appear due to packing constraints. In such a case, the density profile is nonmonotonic in that, the particles in a cavity can be localized in various points forming shells, as in Fig. 3, where  $R=1.25$  and  $\epsilon_w=1.3$ . In this case, two zones of strong localization appear in intermediate points, one close to the origin and the other to the boundary, due to the accumulation of particles in the respective regions, while a very thin liquid drop grows at the origin. The points of strong localization are connected by a very long “bridge,” forming a relatively thick film, with mean density larger than  $\rho(0)$ , and occupying the larger part of the cavity. However, the wall attraction is not strong enough, resulting in a depletion of particles at the wall region [ $\rho(0) > \rho_w$ ], the corresponding branch is decreasingly monotonic and the contact value is an absolute minimum of the density profile, weak wetting.

A similar structure can appear in larger cavities, see Fig. 4, where  $R=6$  and  $\epsilon_w=9$ , where the density profile is also nonmonotonic and corresponds to three branches: The principal one is a thick liquid drop in the origin. The pore wall attracts the particles moderately, thus the corresponding film is not so thick as in strong wetting, and  $\rho_w$  is not much larger than  $\rho(0)$ . Between these two branches there exists a shell,

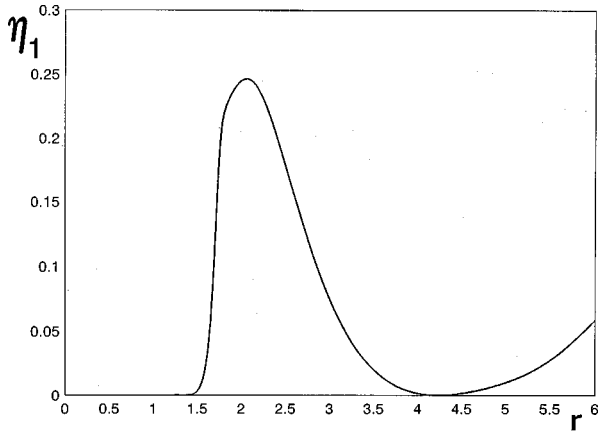


FIG. 4. Density profile  $\eta_1(r)$  vs radial distance  $r$  from the center of a spherical cavity of radius  $R=6$  and wall parameter  $\epsilon_w=9$ . The profile consists of a thick liquid drop in the center, a film at the boundary and a concentric spherical shell close to the cavity's center with a high peak density. The wetting of the boundary is strong,  $\eta_{1w} > \eta_1(0)$ . Both quantities are dimensionless.

closer to the origin, whose peak-density  $\rho_p$  is larger than  $\rho(0)$  and  $\rho_w$ . The thick liquid film in cavity's center results from the strong attractive field  $V_{\text{ext}}(0) = -\epsilon_w R e^{-R}$ , present at  $r=0$  and influenced by  $R$ , in contrast to its value at the boundary where it is constant,  $V_{\text{ext}}(R) \cong -\epsilon_w/2$  and noninfluenced by  $R$ , in the latter case, the boundary behaves as a planar wall [2,12,26].

The variation of the width of the spherical liquid drop formed in the center of the cavity, for various values of  $R$ , can be traced out if we consider its radius  $R_{\text{hom}}$ , Fig. 5.  $R_{\text{hom}}$  is the radius for which the derivative of the density with respect to the radial distance  $r$  vanishes for every  $r < R_{\text{hom}}$ . For small  $R$ 's (smaller or equal to 4) it varies significantly, in some cases is negligible (e.g.,  $R=1.5$  or  $R=4$ ), while it attains a maximum value for  $R=3$ ; for larger  $R$ 's,  $R_{\text{hom}}$  increases steadily, which is an indication that the system becomes equivalent to one with planar substrate instead of spherical.

#### IV. DISCUSSION

The equilibrium local densities and structure of a one-component fluid confined in a spherical cavity and wetting of the boundary have been investigated via density-functional theory considering short-range interactions between the fluid particles and wall fluid; although these interactions do not yield the right physics for any physical system, such a system was found wherein the wetting transition is consistent with the short-range critical wetting [21]. This investigation has pointed out the existence of significant structure inside the cavity, monotonic or nonmonotonic density profiles. Depending on  $R$  and  $\epsilon_w$ , the fluid particles are accumulated not only in the center of the cavity or its boundary, but also in intermediate points, so that the density profile possesses various shells and becomes nonmonotonic, that is, the distribution of the particles of the confined fluid, in some cases,

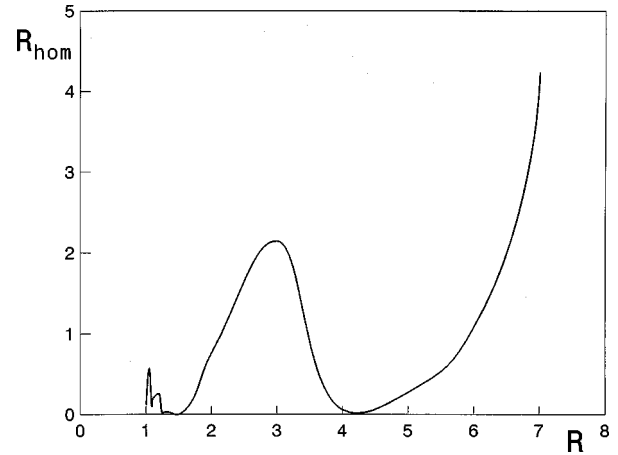


FIG. 5. The radius  $R_{\text{hom}}$  vs the radius  $R$  of the cavity.  $R_{\text{hom}}$  is a measure of the thickness of the liquid drop grown in the center of cavity. It shows significant variation for  $R$  smaller than or equal to 4. Both quantities are dimensionless.

tends to be organized into layered structures, forming concentric spherical shells around the cavity center; this is reflected in the oscillations of the mean local density with radial distance, provided that the boundary is smooth on a molecular scale [27]. The layering can be captured better if a more sophisticated theory is used (smoothed, weighted density approximation [1]), but the behavior found earlier, according to LDA, is an indication that this approximation can capture the qualitative behavior of a system satisfactorily. The radius  $R_{\text{hom}}$  of the drop formed in the center varies from very small values ( $R_{\text{hom}} \ll R$ , see Fig. 5), enclosing a few particles, up to  $R$ , filling the cavity, capillary condensation. The specific case ( $R_{\text{hom}}/R \ll 1$ ) can enclose even one particle (Fig. 5) and corresponds to the so-called quasi-zero-dimensional (0D) situation, wherein the effective dimensionality of the fluid inside the “drop” is reduced drastically and can be assumed as a limiting behavior of a 3D system. The 0D cavity cannot hold more than one particle and this notion can be used for describing the freezing transition [28]. When the confined fluid does not fill the cavity, the central density  $\rho(0)$  varies, in that the peak of the density at  $r=0$  grows with  $\langle N \rangle$  and  $R$  and at this point differences appear between the theoretical and computational results [6].

The drop formed in the center of the cavity imitates a real liquid drop in a vapor background, thus it will exhibit a similar behavior, nevertheless. Its bounding surface is not sharp but undergoes thermally excited surface oscillations, which consist of various modes. The lowest mode corresponds to a translation of the drop through the cavity; because of the absence of a radial stabilizing field (e.g., gravitational), the drop is free to wander throughout the cavity and there is a possibility of the drop to collide with the cavity boundary. The higher modes cause size-dependent phenomena, as is the dependence of the mean-square surface thickness on the logarithm of the drop radius. These surface fluctuations are superimposed on the original surface, which has

an intrinsic thickness, and in an experiment for the measurement of the thickness of the interface it is difficult to separate the intrinsic and capillary components [29].

The surface tension (mechanical and equimolar) and the respective dividing surfaces cannot be defined rigorously because the system consists of a small number of particles; since the number of particles and the radius of the cavity are

finite there cannot be wetting transitions as they appear in a system with a planar wall [12,13].

#### ACKNOWLEDGMENTS

Financial support by the Special Account for Research Grants of the University of Athens (SARG, EAKE) is gratefully acknowledged.

- 
- [1] R. Evans, in *Fundamentals of Inhomogeneous Fluids*, edited by D. Henderson (Dekker, New York, 1992).
- [2] H. T. Davis, *Statistical Mechanics of Phases, Interfaces and Thin Films* (VCH, New York, 1996).
- [3] G. B. Woods, A. Z. Panagiotopoulos, and J. S. Rowlinson, *Mol. Phys.* **63**, 49 (1988).
- [4] A. I. Skoulidas and D. S. Sholl, *J. Chem. Phys.* **113**, 4379 (2000).
- [5] Y. Zhou and G. Stell, *Mol. Phys.* **66**, 767 (1989).
- [6] A. Gonzalez, J. A. White, F. L. Roman, S. Velasco, and R. Evans, *Phys. Rev. Lett.* **79**, 2466 (1997); *J. Chem. Phys.* **109**, 3637 (1998).
- [7] A. K. Macpherson, Y. P. Garignan, and T. Vladimiroff, *J. Chem. Phys.* **87**, 1768 (1987).
- [8] S. Zhou, *J. Chem. Phys.* **110**, 2140 (1999).
- [9] Y. Duda, S. Sokolowski, P. Bryk, and O. Pizio, *J. Phys. Chem. B* **102**, 5490 (1998).
- [10] A. Trokhymchuk, D. Henderson, and S. Sokolowski, *J. Phys. Chem.* **99**, 17 509 (1995).
- [11] A. K. Macpherson, Y. P. Garignan, and T. Vladimiroff, *J. Chem. Phys.* **86**, 4228 (1987).
- [12] I. Hadjiagapiou and R. Evans, *Mol. Phys.* **54**, 383 (1985).
- [13] D. E. Sullivan, *Phys. Rev. B* **20**, 3991 (1979); *J. Chem. Phys.* **74**, 2604 (1981).
- [14] T. Bieker and S. Dietrich, *Physica A* **252**, 86 (1998).
- [15] I. Hadjiagapiou, *J. Phys.: Condens. Matter* **6**, 5303 (1994); **7**, 547 (1995).
- [16] D. Bonn, *Curr. Opin. Colloid Interface Sci.* **6**, 22 (2001).
- [17] P. Tarazona and R. Evans, *Mol. Phys.* **48**, 799 (1983).
- [18] G. F. Teletzke, L. E. Scriven, and H. T. Davis, *J. Chem. Phys.* **77**, 5794 (1982); **78**, 1431 (1983).
- [19] S. Dietrich, in *Phase Transitions and Critical Phenomena*, edited by C. Domb and J. L. Lebowitz (Academic Press, London, 1988), Vol. 12, p. 1.
- [20] M. Schick, in *Proceedings of the Les Houches Summer School, Session XL VIII*, edited by J. Chavrolin, J. F. Joanny, and J. Zinn-Justin (Elsevier, Amsterdam, 1990), p. 415.
- [21] D. Ross, D. Bonn, and J. Meunier, *Nature (London)* **400**, 737 (1999).
- [22] E. Brezin, B. I. Halperin, and S. Leibler, *Phys. Rev. Lett.* **50**, 1387 (1983).
- [23] K. Ragil, J. Meunier, D. Broseta, J. O. Indekeu, and D. Bonn, *Phys. Rev. Lett.* **77**, 1532 (1996).
- [24] N. F. Carnahan and K. E. Starling, *J. Chem. Phys.* **51**, 635 (1969).
- [25] R. H. Nilson and S. K. Griffiths, *J. Chem. Phys.* **111**, 4281 (1999).
- [26] J. S. Rowlinson and B. Widom, *Molecular Theory of Capillarity* (Oxford University Press, Oxford, 1982), Chap. 4.
- [27] Z. T. Németh and H. Löwen, *Phys. Rev. E* **59**, 6824 (1999).
- [28] Y. Rosenfeld, M. Schmidt, H. Löwen, and P. Tarazona, *J. Phys.: Condens. Matter* **8**, L577 (1996); *Phys. Rev. E* **55**, 4245 (1997).
- [29] C. A. Croxton, *Fluid Interfacial Phenomena* (Wiley, New York, 1986).